Three-Dimensional Viscous Analysis of Ducts and Flow Splitters

Walter L. Blackmore* and Craig E. Thompson†
Garrett Turbine Engine Company, Phoenix, Arizona

Until recently, viscous compressible flow solutions have not been sufficiently accurate for practical application to problems associated with internal, three-dimensional duct flow. However, to analyze the effects and predict the losses due to secondary and corner flows in nonaxisymmetric ducts with flow splitters, a fully viscous, three-dimensional compressible flow solution is required. This paper compares the results of the three-dimensional viscous analysis to those of conventional methods and scale-model test data for several mixer-nozzle lobe designs. The comparison demonstrates that this three-dimensional viscous analysis accurately predicts velocity and static-pressure distributions. The analysis also reliably predicts relative ranking with regard to losses. These capabilities enhance design optimization and can provide insight for test program development and reduce program test costs.

Nomenclature

a = local speed of sound
a_{cr} = critical velocity
AR = lobe aspect ratio
C_f = thrust coefficient
C_P = specific heat at constant pressure
h = static enthalpy
h_t' = reference enthalpy
k_e = effective conductivity
L = length
L_{ref} = reference length
P = static pressure
P_{plug} = plug static pressure
P_r = molecular Prandtl number
P_{r_t} = turbulent Prandtl number
P_t' = total pressure
R = radius or gas constant
S = entropy
t = time
T = static temperature
TR = lobe taper ratio
U = viscous velocity
V_{act} = actual velocity
V_{id} = ideal velocity
W = lobe width
W = velocity vector
x = streamwise distance
γ = ratio of specific heats
λ = second coefficient of viscosity
μ = molecular viscosity
μ_e = effective viscosity
μ_t = turbulent component of viscosity
ξ = density ratio
ρ = density
ρ_t' = reference density
ϕ = irrotational velocity potential
Φ = dissipation function
$\bar{\omega}$ = loss coefficient

Introduction

THE internal gas paths of modern turbomachinery often incorporate nonaxisymmetric geometries due to the inclusion of large service struts or flow splitters. In many cases, the flow splitters are followed by irregular nonaxisymmetric ducts. These designs often violate the underlying assumptions of current analytical procedures. For example, radial equilibrium flow analysis is often used to analyze the effects of service struts or radially oriented flow splitters. Some of these techniques set the tangential derivatives equal to zero (i.e., they neglect cross-passage static-pressure gradients and circumferentially average the radially distributed blockage). Some of the later quasi-three-dimensional radial equilibrium solutions[1-6] make an effort to account for the cross-passage terms. This allows the designer to compute surface loadings on the struts or flow splitters as well as midpassage bulk flow properties. However, the duct geometry downstream of the splitter may violate the axisymmetric or periodic assumptions of the radial equilibrium solution.

The nonaxisymmetric splitter duct combination may be analyzed with inviscid three-dimensional flow analysis, which provides both radial and cross-passage pressure and velocity profiles. This leaves the designer with one remaining problem. What is the loss distribution? As in the case of the radial equilibrium solutions, most of the three-dimensional flow solutions are based on a predetermined loss or aerodynamic blockage distribution. Obviously, the most useful tool to the designer is an analysis that not only provides the three-dimensional velocity and pressure gradients, but also provides a realistic prediction of the loss and the secondary or corner flows where most of the loss may be concentrated.

The purpose of this paper is to present results of a solution to the three-dimensional Navier-Stokes equations applied to the primary flow through a mixer nozzle, which is an excellent example of large, blunt-leading-edge flow splitters followed by a nonaxisymmetric duct. The results are compared to test data and conventional analysis methods. The main thrust of the paper is to demonstrate the increased flow visibility and pressure-loss prediction capability of this type of flow analysis. The analysis can provide a guide for optimizing designs and reducing test matrices, thus reducing development time and costs.

Analysis

The technique for numerical solution of the three-dimensional compressible Navier-Stokes equations was previously published by Dodge[7] and compared with turbine cascade flows by Waterman et al.[8] This technique—developed for transonic, viscous, compressible flow—consisted of a separation of the momentum equation. One equation contained shear-force terms, and the other contained pressure forces. The equations remained cross-coupled, suggesting an

Presented as Paper 81-0277 at the AIAA 19th Aerospace Sciences Meeting, St. Louis, Mo., Jan. 12-15, 1981; submitted March 4, 1981; revision received March 23, 1982.

*Supervisor, Installation Aerodynamics Engineering Sciences. Member AIAA.
†Senior Engineer, Installation Aerodynamics Engineering Sciences.

iteration between them. The pressure field and its effect on velocity were solved by a global relaxation solution directly from the continuity equation. The shear-force equation was solved by marching techniques, extensively discussed by Dodge and Lieber.[9] This paper extends the application of the numerical solution to nonaxisymmetric ducts and flow splitters.

The Navier-Stokes equations for turbulent flow are often closed by assuming that an effective viscosity can be used to describe the effects of Reynolds stresses. Based on this assumption, the compressible form can be written as shown in Eq. (1):

$$\rho \frac{DW}{Dt} = -\nabla P + \nabla(\lambda \nabla \cdot W) + \nabla \cdot [\mu_e \text{def} W] \tag{1}$$

where def $W = \nabla W + (\nabla W)^*$, and $(\nabla W)^*$ is the transpose of ∇W.

This equation becomes difficult to solve owing to its extreme nonlinear nature. The selected numerical solution approach is to separate the velocity into its viscous and potential components:

$$W = U + \nabla\phi \tag{2}$$

This separation is made possible by introducing the ideal density:

$$\rho^* = \rho_I'(1 - \nabla\phi\nabla\phi/2h_I')^{1/(\gamma-1)} \tag{3}$$

This allows the pressure gradient to be equated with a totally irrotational term, resulting in the solution momentum equation:

$$\rho(W\cdot\nabla)U + \rho U\cdot\nabla(\nabla\phi) - (\rho^* - \rho)[\nabla\phi\cdot\nabla(\nabla\phi)]$$
$$= \nabla(\lambda\nabla\cdot W) + \nabla\cdot[\mu_e \text{def} W] \tag{4}$$

The second solution equation is derived by combining the continuity equation and the equation of state. This results in the potential equation (5):

$$\nabla\phi\cdot[\nabla\phi\cdot\nabla(\nabla\phi)] - a^2\xi\nabla^2\phi$$
$$= a^2\xi\{\nabla\cdot U + U\cdot\nabla\rho/\rho - [\gamma-1)/\gamma R]\nabla\phi\cdot\nabla S\} \tag{5}$$

where $\xi = \rho/\rho^*$, and $a^2 = (\gamma - 1)h$. The third equation used in the solution is the energy equation. An appropriate energy equation can be given as follows:

$$\rho(W\cdot\nabla)(h + \tfrac{1}{2}W^2) = \nabla\cdot(k_e\nabla T) + \Phi \tag{6}$$

It is convenient to replace the effective conductivity with relationships between density and viscosity:

$$k_e = \mu C_p/P_r + \mu_t C_p/P_{r_t} \tag{7}$$

By assuming that the streamwise diffusion of momentum and thermal energy can be neglected, the momentum equation (4) and the energy equation (6) can be expressed in a parabolic form and solved with a marching technique. The potential equation (5) is solved with a relaxation technique. Since the equations contain coupling terms, an iteration between the marching and relaxation calculations is carried out to arrive at the final solution.

Boundary conditions for Eq. (4) consist of an inlet profile and the no-slip condition at the walls. Thus, at the wall, U is equated to the negative of the potential gradient. The potential boundary conditions [Eq. (5)] can be somewhat more complicated; however, for all cases described herein, an assumption suffices that the gradient of potential normal to the wall is zero. It should be noted that this does not imply that the pressure gradient normal to the wall is zero.

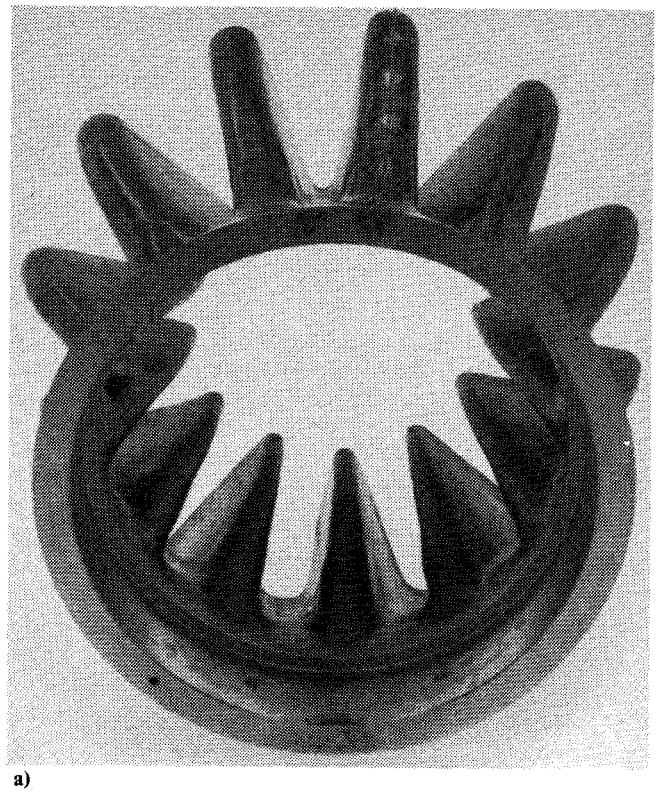

a)

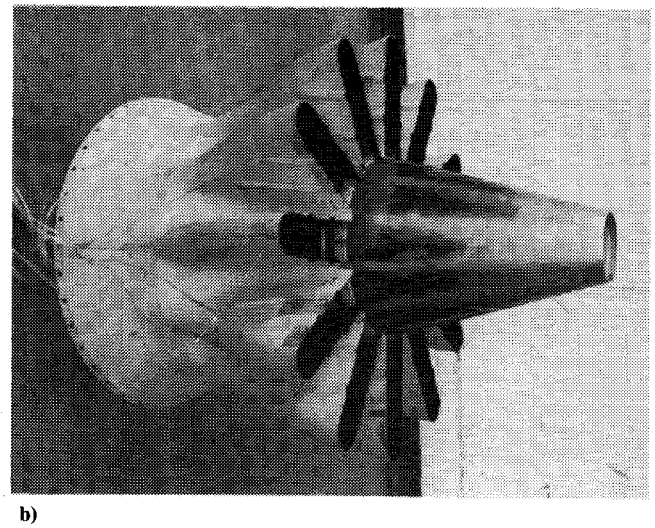

b)

Fig. 1 Core-lobed mixer: a) without plug centerbody and b) with plug centerbody.

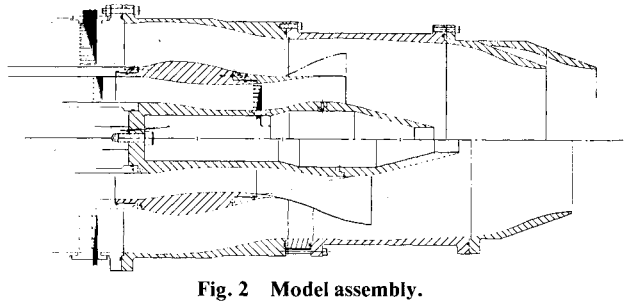

Fig. 2 Model assembly.

Upstream and downstream boundary conditions use a specified constant potential of zero at the inlet and a value based on input data at the exit.

Experiments

The test data used in this paper for analytical comparison are extracted from the AiResearch/NASA Quiet Clean General Aviation Turbofan (QCGAT) (Ref. 10) 0.35 scale-model rig tests.

Data were obtained from model tests on a series of lobed, forced mixers such as shown in Fig. 1. This type of forced mixer is utilized in a turbofan engine in the exhaust nozzle region to mix the high-temperature primary flow with the lower-temperature bypass flow. Mixing of the flows can result in increased thrust if the mixer pressure losses are minimized. Each of the mixer models contained aft-facing base static-pressure taps at the exit and were tested with a centerbody containing wall static-pressure taps. Appropriate rating-station total-pressure and total-temperature rakes were included in each configuration, as shown in Fig. 2 (model assembly sketch).

The mixer loss coefficients presented in this paper were not measured directly, but were derived from measured thrust-coefficient data at different pressure ratio settings. The thrust-coefficient accuracy in the higher-pressure ratio range is ±0.25%, which results in a loss coefficient error of ±20% of value, as shown in Table 1. At the lower-pressure ratio range, the thrust-coefficient accuracy is less—approximately ±0.5%—but the loss coefficient error is slightly improved to ±17% of value owing to an improved loss coefficient/thrust sensitivity factor. For the subsonic flows involved, the loss coefficient for a given configuration is nearly constant; therefore the estimated error in the mean loss coefficient can be reduced by statistical treatment of all the data points for a configuration, i.e.,

$$\frac{\bar{\omega}_{\text{true}}\bar{\omega}_{\text{mean}}}{\bar{\omega}_{\text{true}}} \leq \frac{(\Delta\bar{\omega}/\bar{\omega})_{\max}}{\sqrt{n}}$$

where n is the number of data points.

Using the full 16-point data matrix reduces the deduced loss coefficient error to ±5% of value or less, based on a confidence of 68%.

Table 1 Deduced loss coefficient error

Condition	Thrust coefficient[a] accuracy, ΔC_f	Deduced loss[a] coefficient error, $\Delta\bar{\omega}/\bar{\omega}$
High-pressure ratios, $P_T/P=2.4$	±0.0025	±0.20
Low-pressure ratios, $P_T/P=1.4$	±0.005	±0.17
Overall average	...	±0.05

[a] Numbers based on a confidence of 0.68.

Table 2 Mixer lobe design comparison

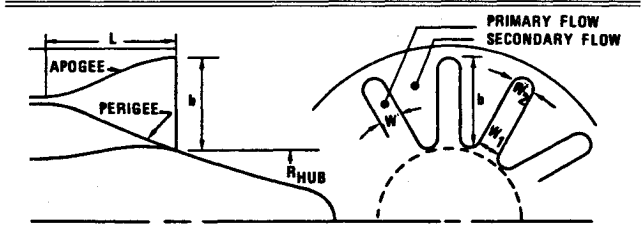

Configuration	Lobe taper ratio, $TR=W_2/W_1$	Lobe aspect ratio, $AR=b/W$	Lobe length ratio, L/L_{ref}
Short parallel	1.0	3.5	1.0
Long parallel	1.0	3.5	1.25
Radial	1.8	3.14	1.25

Three-Dimensional Viscous Analytical Results

Predicted results of three mixer lobe designs are presented because of their relevance to generalized flow splitters and nonaxisymmetric ducts, and owing to the availability of comparative model test data. Each mixer includes swept leading-edge flow splitters with varying maximum thickness. The flow splitters are followed by nonaxisymmetric ducts with three-dimensional accelerating and diffusing flowfields. These three configurations were selected to show the sensitivity of the flow analysis results to moderate geometry change and to demonstrate the relative-pressure-loss prediction capability. The baseline configuration will be denoted as the short-length, parallel-wall, mixer lobe design, referred to as short parallel. The second configuration is a longer scaled version of the baseline design and is referred to as long parallel. The third configuration is the same length as the long parallel, but the lobe walls are radial, the splitter leading edge is thicker, and the apogee and perigee contours are modified. This configuration is designated as the radial design. A summary of the mixer geometries is presented in Table 2.

The internal flow of each mixer was modeled with the three-dimensional viscous flow analysis. An analytical survey plane was cut near the mixer exit in order to study the predicted flowfields. Predicted velocity distributions and loss coefficient contours are presented and discussed in the following section. One of the useful and unique capabilities of the three-dimensional viscous analysis is the ability to predict and study the flowfield effects associated with geometric design variations. This type of analytical flow visibility allows the engineer to design and optimize configurations with velocity and loss distributions that suit his purposes.

Mixer Lobe Exit Velocity Contours

The predicted velocity contours at the lobe exit plane of the three mixer configurations are presented in Fig. 3.

The three-dimensional viscous analysis of the short parallel design shows large diffusion in the tip region with a high-velocity region near the hub. Analysis of the increased length, long parallel design exhibits slightly higher tip diffusion.

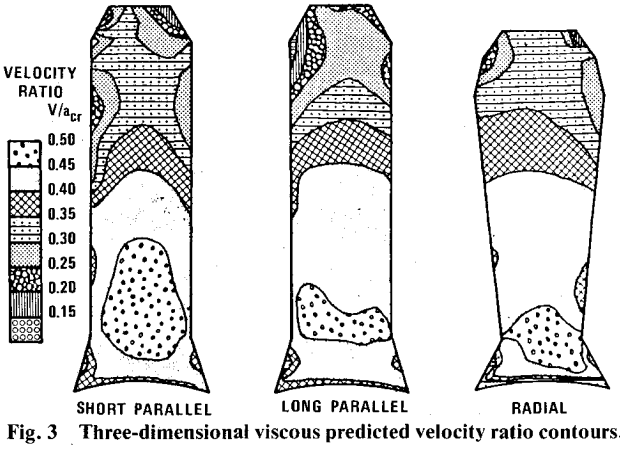

Fig. 3 Three-dimensional viscous predicted velocity ratio contours.

However, the predicted high-velocity regions have penetrated further in the radial direction, and the highest-velocity region is reduced in size. Changing the lobe geometry from the long parallel to the radial design changed the predicted velocity profiles, particularly in the tip region. This is a result of the combined effects of an apogee contour change and an increased flow area at the tip due to a decreased aspect ratio and increased taper ratio. Predicted velocity contours like these provide the designer with a clearer picture of the flowfield. This visibility allows the designer to increase or decrease the velocity profiles and secondary flows. This capability is not available with conventional radial equilibrium or three-dimensional potential flow solutions.

Mixer Lobe Exit Loss Coefficient

Predicted total-pressure-loss contours at the lobe exit plane are presented in Fig. 4. The high-pressure-loss zones correspond to low-velocity regions shown earlier in Fig. 3. The short parallel design exhibits high loss in the tip region, which is attributed to a high rate of local diffusion and corner flow effects. A low-loss region exists in the lower midsection of the lobe and centerbody, and secondary flow losses are exhibited at the hub. By lengthening the lobe to the long parallel configuration, the predicted midchannel losses were reduced considerably; however, the tip-region loss increased. Analysis of the radial wall design showed increased midsection losses, but decreased losses in the upper half of the lobe.

The radial distributions of loss shown in Fig. 5 can be obtained by circumferentially integrating the losses illustrated in Fig. 4. This method of presentation confirms the previously discussed observations. It is obvious that the major sources of loss are in the tip region. This type of analytical visibility allows the engineer to tailor velocity and loss distributions and, consequently, evaluate potential designs relative to each other based on criteria other than an overall loss coefficient.

The predicted overall loss coefficients agree quite well with test data, as shown in Tables 3 and 4. The relative-loss factor presented in Table 3 indicates that the three-dimensional viscous analytical predictions are within 8% of the tested loss. The more traditional radial equilibrium with boundary-layer analysis deviated from the test data by 73%. This large error is due to inability to predict the secondary flow and corner losses. The ranking loss factor of Table 4 demonstrates that within measurement accuracy the three-dimensional viscous analysis is able to accurately predict the ranking according to loss level of the mixer lobe designs.

Axial and Radial Static-Pressure Loadings

Flow properties along a duct wall past a splitter can be studied by combining results from several analytical survey planes. For example, the hub midpassage static-pressure distribution for the short parallel configuration is presented in Fig. 6. For comparative purposes, the rig-test data and

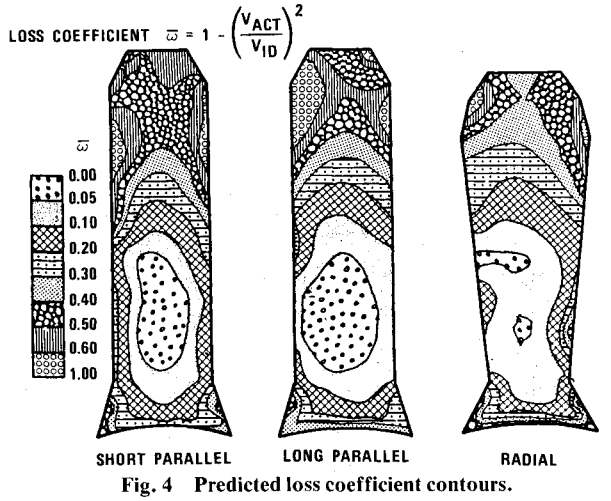

Fig. 4 Predicted loss coefficient contours.

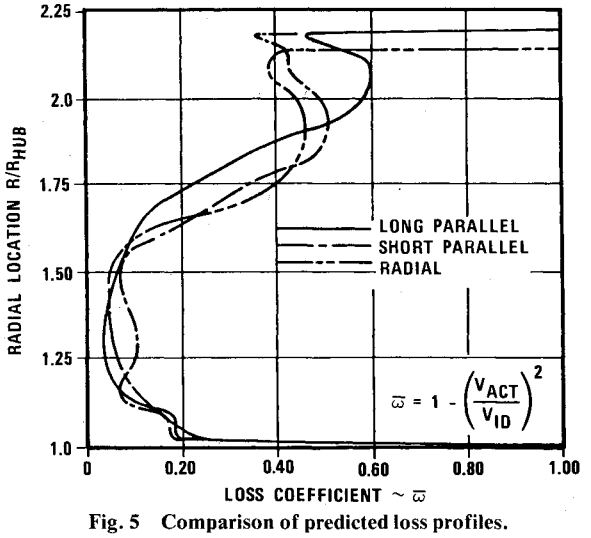

Fig. 5 Comparison of predicted loss profiles.

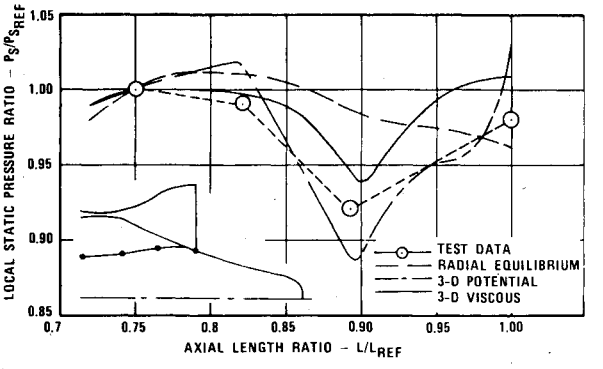

Fig. 6 Hub static-pressure comparisons.

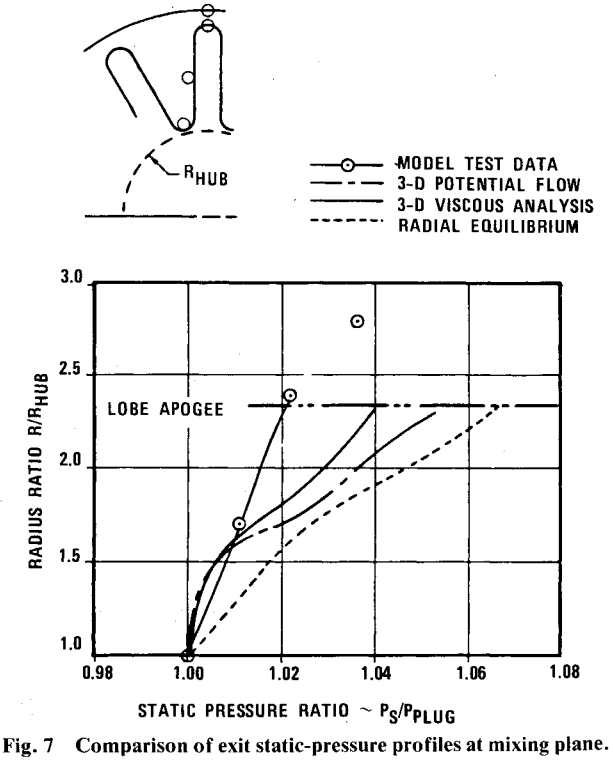

Fig. 7 Comparison of exit static-pressure profiles at mixing plane.

Table 3 Comparison of relative loss change

Configuration	Relative-loss factor ~ $(\bar{\omega}_{pred} - \bar{\omega}_{test})/\bar{\omega}_{test}$ Radial equilibrium with boundary layer	Three-dimensional viscous analysis
Short parallel	−0.73	−0.08
Long parallel	...	0.00
Long radial	...	−0.05

Table 4 Comparison of ranking loss factors

Configuration	Ranking loss factor ~ $(\bar{\omega} - \bar{\omega}_{baseline})/\bar{\omega}_{design}$ Three-dimensional viscous predictions	Test results
Short parallel	0.00	0.00
Long parallel	−0.28	−0.36
Long radial	−0.31	−0.36

computed results from the three-dimensional inviscid flow solution and a radial equilibrium solution are also shown.

The radial equilibrium flow solution with distributed blockage did not predict the acceleration due to lobe blockage as shown by the test data. The three-dimensional potential flow solution overpredicts the acceleration, but, in general, is within ±5% of the test data. Better agreement (±3%) is obtained from the three-dimensional viscous prediction.

Predicted radial static-pressure profiles are compared to test data at the mixer lobe exit plane in Fig. 7. Again the three-dimensional viscous analysis provides the best agreement with test data. At the lobe midspan, the three-dimensional viscous and potential solutions agree very well with the data, while the radial equilibrium solution value is 1.5% higher than the test data. At the apogee, the three-dimensional viscous solution value is 1.8% higher than the data; the three-dimensional potential is 3.2% higher; and the radial equilibrium solution is 4.5% higher. It is believed that the three-dimensional flow solution disagreement near the lobe apogee is due to improperly modeling the boundary conditions established by merging the core and bypass flows near the lobe exit.

Conclusion

An approximate solution to the fully viscous three-dimensional Navier-Stokes equations has been developed which can accurately provide flowfield visibility in three-dimensional ducts and flow splitters and provide relative performance predictions. Comparisons with test data have shown that this type of analysis accurately predicts velocity and static-pressure distributions and produces reliable relative-loss ranking of different three-dimensional duct systems.

Use of this type of analysis can significantly reduce design and development costs by reducing the number of required test configurations and by providing early performance information on potential designs.

References

[1] Smith, L.H. Jr., "The Radial-Equilibrium Equation of Turbomachinery," *Journal of Engineering for Power,* Vol. 88, Jan. 1966, pp. 1-12.

[2] Hirsch, C.H. and Warzee, G., "A Finite Element Method for Through-Flow Calculations in Turbomachines," ASME Paper 76-FE-12, March 1976.

[3] Novak, R.A. and Hearsey, R.M., "A Nearly Three-Dimensional Intrablade Computing System for Turbomachinery—Part I: General Description," ASME Paper 76-FE-19, March 1976.

[4] Novak, R.A. and Hearsey, R.M., "A Nearly Three-Dimensional Intrablade Computing System for Turbomachinery—Part II: System Details and Additional Examples," ASME Paper 76-FE-20, March 1976.

[5] Biniaris, S., "The Calculation of the Quasi-Three-Dimensional Flow in an Axial Gas Turbine," ASME Paper 74-GT-67, Nov. 1973.

[6] Bosman, C. and El-Shaarawi, M.A.I., "Quasi-Three-Dimensional Numerical Solution of Flow in Turbomachines," ASME Paper 76-FE-23, March 1976.

[7] Dodge, P.R., "Numerical Method for 2-D and 3-D Viscous Flows," *AIAA Journal,* Vol. 15, July 1977, pp. 961-965.

[8] Waterman, W.F. and Tall, W.A., "Measurements and Prediction of 3-D Viscous Flows in Low-Aspect-Ratio Turbine Nozzles," ASME Paper 76-GT-73, March 1976.

[9] Dodge, P.R. and Lieber, L.S., "A Numerical Method for the Solution of the Navier-Stokes Equations with Separated Flows," AIAA Paper 77-170, Jan. 1977.

[10] Blackmore, W.L. and Thompson, C.E., "QCGAT Mixer Compound Exhaust System Design and Static Rig Model Test Report," NASA CR-135386, Oct. 1978.